Initial state dependence of the quench dynamics in integrable quantum systems. III. Chaotic states

Kai He[1,2] and Marcos Rigol[1]

[1] *Department of Physics, The Pennsylvania State University, University Park, Pennsylvania 16802, USA*
[2] *Department of Physics, Georgetown University, Washington, DC 20057, USA*

We study sudden quantum quenches in which the initial states are selected to be either eigenstates of an integrable Hamiltonian, which is non-mappable to a noninteracting one, or a nonintegrable Hamiltonian while the Hamiltonian after the quench is always integrable (and mappable to a noninteracting one). By studying weighted energy densities and entropies, we show that quenches starting from the nonintegrable (chaotic) eigenstates lead to an "ergodic" sampling of the eigenstates of the final Hamiltonian, while those starting from the integrable eigenstates do not (at least for the system sizes accessible to us). This goes in parallel with the fact that the distribution of conserved quantities in the initial states is thermal in the nonintegrable cases and nonthermal in the integrable ones, and means that, in general, thermalization occurs in integrable systems when the quench starts from an eigenstate of a nonintegrable Hamiltonian (away from the edges of the spectrum), while it fails (or requires much larger system sizes) for quenches starting at integrable points that are non-mappable to free models. We test those conclusions by studying the momentum distribution function of hard-core bosons after a quench.

PACS numbers: 02.30.Ik,05.30.-d,03.75.Kk,05.30.Jp

I. INTRODUCTION

The experimental realization of ultracold quantum gases in (quasi-)one-dimensional (1D) geometries has stimulated much theoretical research on 1D systems [1]. In equilibrium, they are particularly interesting because of the enhanced role played by quantum fluctuations. In addition, when taken out of equilibrium, they may exhibit unique behavior such as lack of thermalization [2, 3]. We note that those systems are well isolated by the ultra high vacuum in which they are confined, i.e., their dynamics is to a very good approximation unitary [4]. Hence, by lack of thermalization we mean the fact that, after perturbing the system and letting it evolve, experimental observables relax to time-independent values that are not described by conventional statistical ensembles. This effect has been attributed to the proximity to integrable points [5–8], and has motivated an extensive exploration of the dynamics of integrable systems [8–27].

The most common dynamics studied in this context are the ones that occur after the so-called sudden quenches. In a sudden quench, the initial state $|\Psi_I\rangle$ is selected to be an eigenstate $|\phi_n\rangle$ of an initial Hamiltonian $\hat{H}_I$ ($\hat{H}_I|\phi_n\rangle = \epsilon_n|\phi_n\rangle$). Then, at time $\tau = 0$, some parameter(s) of $\hat{H}_I$ is(are) changed instantaneously $\hat{H}_I \to \hat{H}_F$, and the dynamics is followed under the final (time-independent) Hamiltonian $\hat{H}_F$ ($\hat{H}_F|\psi_\alpha\rangle = E_\alpha|\psi_\alpha\rangle$)

$$|\Psi(\tau)\rangle = e^{-i\hat{H}_F\tau/\hbar}|\Psi_I\rangle = \sum_\alpha C_\alpha e^{-iE_\alpha\tau/\hbar}|\psi_\alpha\rangle, \quad (1)$$

where $C_\alpha = \langle\psi_\alpha|\Psi_I\rangle$ are the overlaps of the initial state with the eigenstates of the final Hamiltonian.

Within this protocol, the time evolution of the expectation value of an observable $\hat{O}$, $\langle\hat{O}(\tau)\rangle = \langle\Psi(\tau)|\hat{O}|\Psi(\tau)\rangle$, can be written as

$$\langle\hat{O}(\tau)\rangle = \sum_\alpha |C_\alpha|^2 O_{\alpha\alpha} + \sum_{\alpha\neq\beta} C^*_\alpha C_\beta e^{i(E_\alpha - E_\beta)\tau/\hbar} O_{\alpha\beta}, \quad (2)$$

where $O_{\alpha\beta} = \langle\psi_\alpha|\hat{O}|\psi_\beta\rangle$. If the observable relaxes to a time-independent value (up to fluctuations that vanish and revival times that diverge in the thermodynamic limit), that value can be computed (up to corrections that vanish in the thermodynamic limit) by taking the infinite-time average of Eq. (2)

$$\begin{aligned}\overline{\langle\hat{O}(\tau)\rangle} &= \lim_{\tau'\to\infty}\frac{1}{\tau'}\int_0^{\tau'} d\tau\,\langle\hat{O}(\tau)\rangle \\ &= \sum_\alpha |C_\alpha|^2 O_{\alpha\alpha} \equiv \langle\hat{O}\rangle_{\rm DE}, \end{aligned} \quad (3)$$

where we have assumed that there are no degeneracies, or that they can be neglected. The infinite-time average can be thought of as the prediction of an ensemble, the "diagonal ensemble" [8], where the density matrix is diagonal in the basis of eigenstates of the final Hamiltonian, i.e., $\hat{\rho}_{\rm DE} = \sum_n |C_\alpha|^2 |\psi_\alpha\rangle\langle\psi_\alpha|$.

Several theoretical studies have shown that in integrable systems, and for observables of interest in current experiments and models, $\langle\hat{O}\rangle_{\rm DE}$ is different from the predictions of conventional statistical mechanics ensembles [8–10, 18, 25, 26]. Among the (few-body) observables that have been studied are the density and momentum distribution function of hard-core bosons [8–10], the double occupancy of fermions [18], and spin-spin correlations in spin chains [25, 26]. If one wants to go beyond conventional statistical mechanics ensembles to take into account that nontrivial conserved quantities $\{\hat{I}_j\}$ (whose number scales polynomially with system size) are present in integrable systems, and maximizes the entropy under

those constraints [28, 29], then a generalized Gibbs ensemble (GGE) is obtained [8]. Remarkably, the GGE has been shown to provide the correct description for the previously mentioned observables (and others) after relaxation following a sudden quench [8–10, 13–18, 24–26]. The (grand-canonical) density matrix for the GGE can be written as [8]

$$\hat{\rho}_{\rm GGE} = \frac{1}{Z_{\rm GGE}} e^{-\sum_j \lambda_j \hat{I}_j}, \tag{4}$$

where $Z_{\rm GGE} = {\rm Tr}[e^{-\sum_j \lambda_j \hat{I}_j}]$ is the partition function, $\hat{I}_j$ are conserved quantities, and λ_j are their corresponding Lagrange multipliers. The latter are computed using that $\langle \Psi_I | \hat{I}_j | \Psi_I \rangle = {\rm Tr}[\hat{\rho}_{\rm GGE}\, \hat{I}_j]$.

The lack of thermalization of few-body observables of interest in integrable systems has been attributed to the failure of the eigenstate thermalization hypothesis [5–7, 10, 30, 31]. That is to say that, within a microcanonical window, the matrix elements $O_{\alpha\beta}$ in an integrable system fluctuate over a finite range of values. Hence, the outcome of the quench dynamics depends on which eigenstates of the final Hamiltonian have a finite overlap with the initial state. If the initial state samples the eigenstates within the microcanonical window in an unbias way, i.e., "ergodically", then for that initial state the integrable system will thermalize. This does not happen for most quenches between integrable systems studied in the literature [8–10, 13–15, 17, 18, 24–26]. However, it has been shown to occur for special initial states [11] with particular entanglement properties [16], as well as for initial thermal states at infinite temperature [12]. In the latter work, finite temperatures were shown to lead to a bias sampling of the final eigenstates of the Hamiltonian after a quench.

In this work, we study what happens in quenches from initial states that are eigenstates of an integrable Hamiltonian that is non-mappable to a noninteracting one, while the final Hamiltonian is integrable (and mappable to a noninteracting one). This is of interest as most studies in the literature have focused on quenches where both the initial and final Hamiltonians are mappable to noninteracting ones. We also study the case in which the initial state is an eigenstate of a nonintegrable Hamiltonian and the final Hamiltonian is integrable. As argued in Ref. [32], initial states that are eigenstates of nonintegrable Hamiltonians (away from the edges of the spectrum) can lead to thermalization even though the final Hamiltonian is integrable. This can be understood as the two-body interactions that break integrability in models of current interest lead to quantum chaos even in the absence of randomness [33–36], similar to what happens in systems with two-body random interactions [37–40]. As a result, the eigenstates of nonintegrable Hamiltonians become random superpositions of eigenstates of the integrable ones to which the quench is performed, i.e., they provide the un-bias sampling required for thermalization after a quench to integrability. We do not find indications that this happens in quenches between the integrable systems studied here.

The exposition is organized as follows. In Sec. II, we introduce the model Hamiltonian and describe the quenches to be studied. The observables and ensembles of interest are introduced in Sec. III. The remainder sections are devoted to the discussion of the results for: (i) overlaps between initial states and eigenstates of the final Hamiltonians (Sec. IV), (ii) entropies (Sec. V), (iii) conserved quantities (Sec. VI), and (iv) momentum distribution functions (Sec. VII). A summary of the results is presented in Sec. VIII.

II. MODEL HAMILTONIAN AND QUENCHES

We focus our study on 1D lattice hard-core bosons in a box (a system with open boundary conditions) with nearest-neighbor (NN) hopping t and interaction V, and next-nearest-neighbor (NNN) hopping t' and interaction V'. The Hamiltonian reads

$$\hat{H} = \sum_{i=1}^{L-1} -t(\hat{b}_i^\dagger \hat{b}_{i+1} + {\rm H.c.}) + V\left(\hat{n}_i - \frac{1}{2}\right)\left(\hat{n}_{i+1} - \frac{1}{2}\right) + \sum_{i=1}^{L-2} -t'(\hat{b}_i^\dagger \hat{b}_{i+2} + {\rm H.c.}) + V'\left(\hat{n}_i - \frac{1}{2}\right)\left(\hat{n}_{i+2} - \frac{1}{2}\right), \tag{5}$$

where $\hat{b}_i^\dagger (\hat{b}_i)$ is the hard-core boson creation (annihilation) operator, $\hat{n}_i = \hat{b}_i^\dagger \hat{b}_i$ the number operator, and L is the lattice size. In addition to the usual commutation relations $[\hat{b}_i, \hat{b}_j^\dagger] = \delta_{ij}$, $\hat{b}_i^\dagger$ and $\hat{b}_i$ satisfy the constraints $\hat{b}_i^{\dagger 2} = \hat{b}_i^2 = 0$, which preclude multiple occupancy of the lattice sites. In what follows, the NN hopping parameter sets the energy scale ($t = 1$), we take $\hbar = k_B = 1$ (where k_B is the Boltzman constant), and the number of particles N is always selected to be $N = L/3$.

For $t' = V' = 0$, Hamiltonian (5) is integrable (it can be mapped onto the spin-1/2 XXZ chain) [1]. In addition, if $V = 0$, the model can be exactly solved by first being mapped onto the spin-1/2 XY chain through the Holstein-Primakoff transformation [41] and then onto noninteracting fermions by means of the Jordan-Wigner transformation [42]. Hence, the many-body eigenstates of the fermionic counterpart are Slater determinants. Properties of Slater determinants allow one to calculate off-diagonal correlations of hard-core bosons in polynomial time for both pure states [43–45] and the grand-canonical ensemble [46]. The presence of nonzero NNN terms break the integrability of the model and drive the system to a chaotic regime [33–36].

Here, we consider two types of quenches. Quench type I is within integrable models, i.e, we keep $t' = V' = 0$ at all times, and select the initial state to be an eigenstate of Hamiltonian (5) with $V_I > 0$, while the evolution is studied under Hamiltonian (5) with $V_F = 0$. Quench type II is from a nonintegrable model to an integrable one:

namely, the initial state is selected to be an eigenstate of Hamiltonian (5) with $t'_I = V'_I \neq 0$ while the dynamics is studied under Hamiltonian (5) with $t'_F = V'_F = 0$. In Quench type II, we keep $V = 0$ at all times. Note that the final Hamiltonian in both types of quenches is the same. It can be fully diagonalized for large systems by being mapped onto noninteracting fermions as mentioned before. In addition, since $V \neq 0$ and $t' = V' \neq 0$ are only present in the initial Hamiltonian, in what follows we drop the sub-index "I" from V_I and $t'_I = V'_I$.

In order to compare results of quenches from eigenstates of different initial Hamiltonians, we select the initial states $|\Psi_I\rangle$ such that after the quench the systems have an energy

$$E_I = \langle \Psi_I | \hat{H}_F | \Psi_I \rangle, \tag{6}$$

which always corresponds to that of the canonical ensemble (CE) at a fixed temperature $T_{\rm CE}$ (the temperature is taken to be $T_{\rm CE} \approx 2$ throughout this work). This means that $E_I = {\rm Tr}\{\hat{\rho}_{\rm CE}\, \hat{H}_F\}$, where $\hat{\rho}_{\rm CE} = e^{-\hat{H}_F/T_{\rm CE}}/Z_{\rm CE}$ is the CE density matrix, and $Z_{\rm CE} = {\rm Tr}\{e^{-\hat{H}_F/T_{\rm CE}}\}$ is the partition function. The initial states, which are eigenstates of the t-V and t-t'-V' models, i.e., none of which is mappable to a free model, are computed by means of the FILTLAN package that utilizes a polynomial filtered Lanczos procedure [47]. Since open boundary conditions are imposed, the only remaining symmetry at 1/3 filling and for $V < 2$, is parity. Here, we restrict our analyses to the even parity sectors, the dimension of which is about 1/2 of the entire Hilbert space. The largest systems we study have $L = 24$, whose total Hilbert space dimension is $D = \binom{24}{8} = 735\ 471$. The even parity subspace for those systems has dimension $D_{\rm even} = 367\ 983$. This is more than ten times larger than the largest Hamiltonian sector diagonalized in previous full exact diagonalization studies of similar systems [6, 7, 33–36]. In this work, the combination of utilizing Lanczos algorithm for computing the initial state, and full exact diagonalization via the Bose-Fermi mapping for the final Hamiltonian, is what allows us to perform a complete analysis for larger Hilbert spaces.

III. ENSEMBLES AND OBSERVABLES

Given the fact that the initial states ($|\Psi_I\rangle$) are pure states, and that the dynamics is unitary, the von Neumann entropy is zero at all times. In order to characterize our isolated systems, we make use of the diagonal entropy $S_{\rm DE}$. It is defined as the von Neumann entropy of the diagonal ensemble [48]

$$S_{\rm DE} = -\sum_{\alpha} |C_\alpha|^2 \ln\left(|C_\alpha|^2\right), \tag{7}$$

and satisfies all thermodynamic properties expected of an entropy [48]. $S_{\rm DE}$ has been recently shown to be consistent with the entropy of thermal ensembles for generic (nonintegrable) systems after relaxation [49].

Similar to the studies in Refs. [11, 12], we compare the DE with the entropy predicted by the CE, the grand-canonical ensemble (GE), and the GGE. Namely, we also compute

$$S_{\rm CE} = \ln Z_{\rm CE} + \frac{E_I}{T_{\rm CE}}, \tag{8}$$

$$S_{\rm GE} = \ln Z_{\rm GE} + \frac{E_I - \mu N}{T_{\rm GE}}, \tag{9}$$

$$S_{\rm GGE} = \ln Z_{\rm GGE} + \sum_j \lambda_j \langle \Psi_I | \hat{I}_j | \Psi_I \rangle, \tag{10}$$

where E_I was defined in Eq. (6), and $Z_{\rm CE}$, $T_{\rm CE}$, N, and $Z_{\rm GGE}$ were also defined before. In Eq. (9), the chemical potential and the temperature are computed such that $E_I = {\rm Tr}[\hat{\rho}_{\rm GE}\, \hat{H}_F]$ and $N = {\rm Tr}[\hat{\rho}_{\rm GE}\, \hat{N}]$, where $\hat{\rho}_{\rm GE} = e^{-(\hat{H}_F - \mu\hat{N})/T_{\rm GE}}/Z_{\rm GE}$ is the GE density matrix, $Z_{\rm GE} = {\rm Tr}\{e^{-(\hat{H}_F - \mu\hat{N})/T_{\rm GE}}\}$ is the partition function, and $\hat{N}$ is the total number of particle operator.

As mentioned before, all our quenches share the same final Hamiltonian ($V = t' = V' = 0$), which is integrable. The conserved quantities $\{\hat{I}_j\}$ for the GGE in that model are taken to be the occupation number operators of the single particle eigenstates of the fermionic Hamiltonian to which hard-core bosons can be mapped. From this selection, it follows straightforwardly that the corresponding Lagrange multipliers can be computed as $\lambda_j = \ln[(1 - \langle \Psi_I | \hat{I}_j | \Psi_I \rangle)/\langle \Psi_I | \hat{I}_j | \Psi_I \rangle]$ [8]. Note that, by construction, the GGE has the same distribution of conserved quantities as the diagonal ensemble. We also calculate the distribution of conserved quantities predicted by the GE, namely, $\langle \hat{I}_j \rangle_{\rm GE} = {\rm Tr}[\hat{\rho}_{\rm GE}\, \hat{I}_j]$.

In addition, we study the momentum distribution function of hard-core bosons in the DE ($\langle \hat{m}_k \rangle_{\rm DE} = {\rm Tr}[\hat{\rho}_{\rm DE}\, \hat{m}_k]$), the GE ($\langle \hat{m}_k \rangle_{\rm GE} = {\rm Tr}[\hat{\rho}_{\rm GE}\, \hat{m}_k]$), and the GGE ($\langle \hat{m}_k \rangle_{\rm GGE} = {\rm Tr}[\hat{\rho}_{\rm GGE}\, \hat{m}_k]$). $\hat{m}_k$ is the diagonal part of the Fourier transform of the one-particle density matrix operator $\hat{\rho}_{ij} = \hat{b}_i^\dagger \hat{b}_j$,

$$\hat{m}_k = \frac{1}{L} \sum_{i,j=1}^{L} e^{{\rm i}k(i-j)}\, \hat{\rho}_{ij}. \tag{11}$$

and it was previously studied in systems out of equilibrium with the same $\hat{H}_F$ in Refs. [8–10].

IV. OVERLAPS

As mentioned before, in integrable systems, the lack of eigenstate thermalization implies that the distribution of overlaps of the initial state with the eigenstates of final Hamiltonian $|C_\alpha|^2$ plays a very important role in determining the expectation value of observables after relaxation [Eq. (2)]. Therefore, we first study the values of $|C_\alpha|^2$ as a function of E_α in quenches type I and type II and compare them to the weights of the eigenstates of the final Hamiltonian in the CE, $e^{-E_\alpha/T_{\rm CE}}/Z_{\rm CE}$.

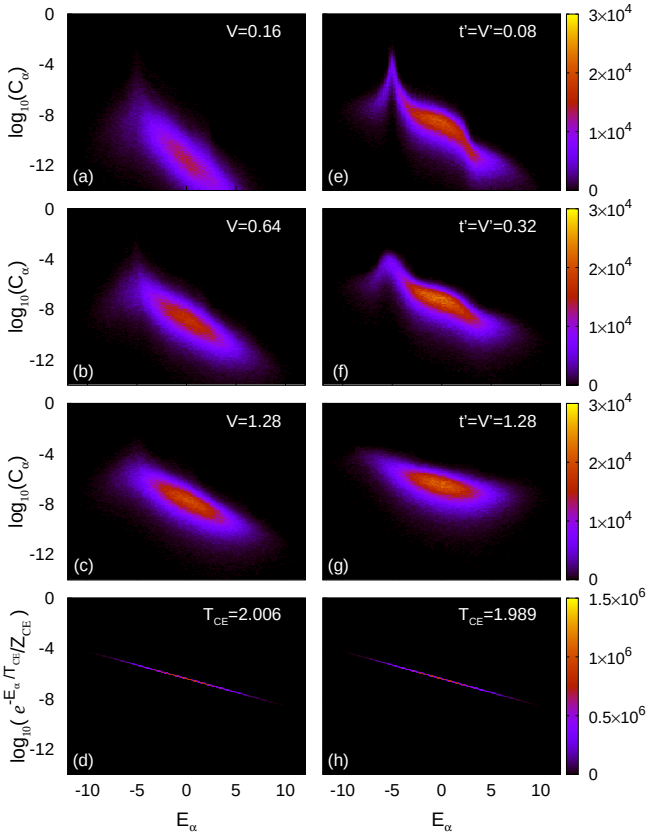

FIG. 1: (Color online) Coarse-grained plot of the weights in the DE [(a)–(c), (e)–(g)], and in the CE [(d) and (h)], $|C_\alpha|^2$ and $e^{-E_\alpha/T_{\rm CE}}/Z_{\rm CE}$, respectively. (a)–(c) Results for quench type I for different values of V. (e)–(g) Results for quench type II with different values of $t' = V'$. (d) and (h) Weights in the CE, which correspond to effective temperatures $T_{\rm CE} = 2.006$ ($E_I = -4.976$) and $T_{\rm CE} = 1.989$ ($E_I = -5.011$), obtained for the quenches with $V = 1.28$ and $t' = V' = 1.28$, respectively. All results are for $L = 24$, $N = 8$, and the temperatures are $T_{\rm CE} = 2.00 \pm 0.01$. The color scale indicates the number of states per unit area in the plot.

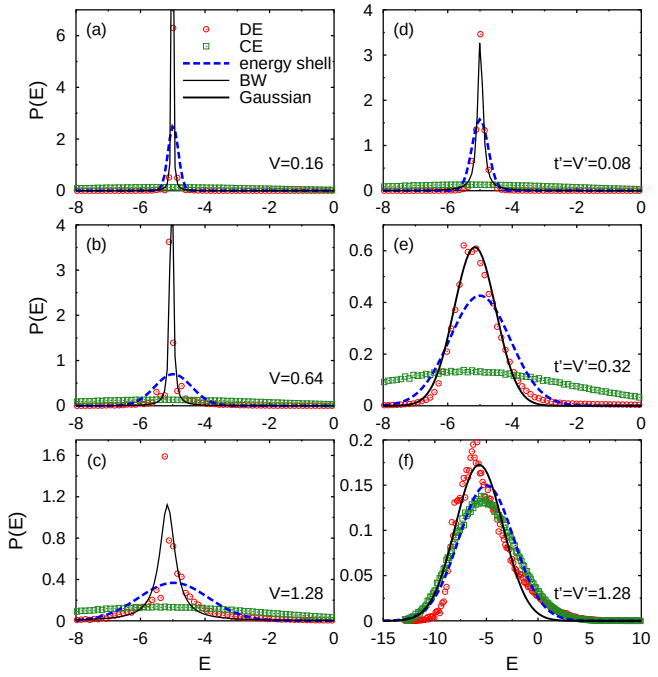

FIG. 2: (Color online) Weighted energy density functions $P(E)$ for both the DE and the CE. (a)–(c) Results for quenches type I. (e)–(f) Results for quenches type II. The dashed (blue) lines depict the energy shell, where (a) $E_I = -4.99$, $\delta E = 0.159$, (b) $E_I = -4.99$, $\delta E = 0.571$, (c) $E_I = -4.98$, $\delta E = 1.08$, (d) $E_I = -5.00$, $\delta E = 0.253$, (e) $E_I = -5.00$, $\delta E = 0.936$, and (f) $E_I = -5.01$, $\delta E = 2.66$. Solid lines show the results of the fits of $P(E)$ to the most appropriate functional form. Thin lines are fits to a Breit-Wigner function with (a) $\overline{E} = -5.01$, $\Gamma = 0.042$, (b) $\overline{E} = -5.04$, $\Gamma = 0.101$, (c) $\overline{E} = -5.17$, $\Gamma = 0.567$, (d) $\overline{E} = -4.99$, $\Gamma = 0.187$, while thick lines are fits to a Gaussian with (e) $\overline{E} = -5.16$, $\Delta = 0.650$, and (f) $\overline{E} = -5.70$, $\Delta = 2.31$. In all cases $L = 24$ and $N = 8$.

In Fig. 1, we show density plots of the coarse-grained values of $|C_\alpha|^2$ for different quenches type I [Figs. 1(a)–1c)] and type II [Figs. 1(e)–1(h)]. The corresponding results for the canonical weights ($T_{\rm CE} \approx 2$) are presented in Figs. 1(d) and 1(h). One can clearly see in Fig. 1 that, for all values of V in quench type I and $t' = V'$ in quench type II, the distribution of weights in the DE is qualitatively distinct from that in the CE, which shows a simple exponential decay. In the diagonal ensemble, the weights between eigenstates that are close in energy fluctuate wildly (note the logarithmic scale in the y axes), and a maximum in the values of $|C_\alpha|^2$ [particularly clear in panels (a), (b), (e) and (f)] can be seen around the energy of the initial state after the quench $E_I \approx -5.0$. Hence, in contrast to the canonical ensemble, eigenstates of $\hat{H}_F$ whose energies are close to E_I usually have the largest weights. This was also seen in Ref. [50].

Another feature that is apparent in Fig. 1 is that while the weights $|C_\alpha|^2$ decrease rapidly as one moves away from E_I, the number of states with those weights increases dramatically for $E_\alpha > E_I$ due to the increase of the density of states. For this reason, the appropriate quantity to quantify how different regions of the spectrum contribute to the observables in the diagonal ensemble (and in the CE) is the weighted energy density function

$$P(E) = \frac{1}{\Delta E} \sum_{|E-E_\alpha|<\Delta E/2} W_\alpha, \qquad (12)$$

where W_α is $|C_\alpha|^2$ for the DE and $e^{-E_\alpha/T_{\rm CE}}/Z_{\rm CE}$ for the CE. The summation is limited to the states in a small energy window $|E - E_\alpha| < \Delta E/2$, the width of which ΔE is selected to be the same for coarse-graining in Fig. 1. We have checked that our results are robust for the selected values of ΔE.

The weighted energy density functions for the quenches studied in Fig. 1 are shown in Fig. 2. There one can see that in all cases, except for the strongest type

II quenches, $P(E)$ in the CE is much broader than that in the DE. For comparison, we have also plotted the results for the energy shells, which are Gaussians $(\sqrt{2\pi}\delta E)^{-1}\exp[-(E-E_I)^2/(2\delta E^2)]$ with the same mean energy E_I and energy width $\delta E^2 = \sum_\alpha |C_\alpha|^2 (E_\alpha - E_I)^2$ as the diagonal ensemble. The energy shell has the maximal number of eigenstates of the final Hamiltonian that is accessible to the particular initial state selected. In quenches type I [Figs. 2(a)-2(c)], even for the largest V, $P(E)$ in the diagonal ensemble remains narrower than the energy shell. This is an indication of the lack of "ergodicity" of the initial states associated with quench type I. On the contrary, in quenches type II [Figs. 2(d)-2(f)], the width of $P(E)$ in the diagonal ensemble approaches that of the energy shell with increasing $t' = V'$. For the strongest quench considered, $t' = V' = 1.28$, $P(E)$ in the DE and the CE become very close to each other as well as to the energy shell [Fig. 2(f)]. The latter shows that initial states that are eigenstates of nonintegrable Hamiltonians sufficiently distant from an integrable point fill the energy shell ergodically after a quench to integrability.

To better characterize $P(E)$ as one goes from the weakest to the strongest quenches, we have fitted it to two different functions: (i) a Breit-Wigner function

$$P(E) = \frac{1}{2\pi}\frac{\Gamma}{(E-\overline{E})^2 + (\Gamma/2)^2}, \tag{13}$$

and (ii) a Gaussian

$$P(E) = \frac{1}{\sqrt{2\pi}\Delta}\exp\left[\frac{-(E-\overline{E})^2}{2\Delta^2}\right], \tag{14}$$

where the mean energy $\overline{E}$ and half-width Γ of the Breit-Wigner function, as well as the mean energy $\overline{E}$ and half-width Δ of the Gaussian, are taken as fitting parameters.

Figures 2(a)-2(c) show that, as the strength of the interaction increases in quenches type I, the weighted energy densities in the DE are better described by Breit-Wigner functions. In quenches type II [Figs. 2(d)-2(f)], on the other hand, weighted energy densities are described by Breit-Wigner functions for weak quenches and transition to Gaussians as the strength of the quench increases. The fact that $P(E)$ in the latter quenches approach Gaussians (and ultimately the energy shell) hints the possibility of observing thermalization in those cases. This is consistent with the results in Refs. [35, 36], which considered a different set of quench protocols and were averaged over different initial states. Note that, in our results, no average has been introduced.

Using the Breit-Wigner function to fit the weighted energy densities for the weakest quenches of type II, as well as the quenches of type I, is motivated by analytic results obtained in the random two-body interaction model [37–40], and by recent numerical results for models similar to those considered here [35, 36]. In Refs. [35, 36], the weighted energy densities (called strength functions) were computed for quenches that were the reverse from those considered here, namely, starting from a state $|\Phi\rangle$ that is an eigenstate $|\psi_\alpha\rangle$ of an integrable Hamiltonian (in one case, our $\hat{H}_F$) and projecting that state onto the eigenstates $|\phi_n\rangle$ of the t-V and t-t'-V' Hamiltonians (our $\hat{H}_I$), i.e., $|\Phi\rangle = \sum_n c_n |\phi_n\rangle$. In our notation, the weighted energy densities from those works can be written as

$$P(\epsilon) = \frac{1}{\Delta\epsilon}\sum_{|\epsilon-\epsilon_n|\le\Delta\epsilon/2} |c_n|^2, \tag{15}$$

where the sum runs over states in the spectrum of $\hat{H}_I$ within a small window of energy $\Delta\epsilon$. Correspondingly, the energy shell associated with $P(\epsilon)$ is now a Gaussian centered at $\epsilon_S = \sum_n |c_n|^2 \epsilon_n$ whose width is $\delta\epsilon = \sum_n |c_n|^2 (\epsilon_n - \epsilon_S)^2$.

For chaotic systems, it was shown in Refs. [35–40], that as the interaction strength increases, and the average strength of the coupling between unperturbed eigenstates becomes of the order of the average unperturbed level spacing, $P(\epsilon)$ transitions from a Breit-Wigner function to a Gaussian. This transition also seen numeri-

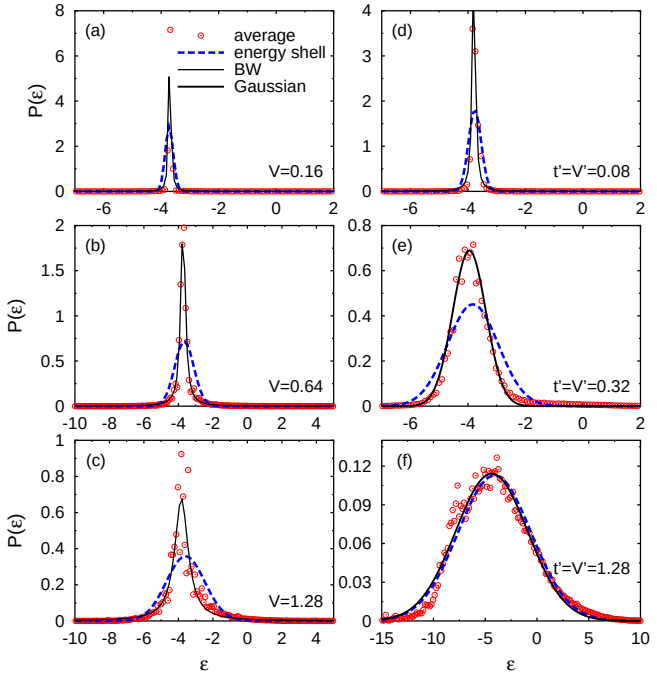

FIG. 3: (Color online) $P(\epsilon)$ for (a)–(c) type I quenches and (d)–(f) type II quenches. They were obtained by averaging over the nine even states $|\psi_\alpha\rangle$ that are closest in energy to E_I. Before averaging, we shift ϵ_S of each distribution to the one obtained for the state $|\psi_\alpha\rangle$ that is closest in energy to E_I. The dashed (blue) lines depict the energy shell, where (a) $\epsilon_S = -3.72$, $\delta\epsilon = 0.139$, (b) $\epsilon_S = -3.66$, $\delta\epsilon = 0.557$, (c) $\epsilon_S = -3.59$, $\delta\epsilon = 1.11$, (d) $\epsilon_S = -3.76$, $\delta\epsilon = 0.221$, (e) $\epsilon_S = -3.83$, $\delta\epsilon = 0.885$, and (f) $\epsilon_S = -4.10$, $\delta\epsilon = 3.54$. Solid lines show the results of the fits of $P(\epsilon)$ to the most appropriate functional form. Thin lines are fits to a Breit-Wigner function with (a) $\overline{\epsilon} = -3.70$, $\Gamma = 0.074$, (b) $\overline{\epsilon} = -3.79$, $\Gamma = 0.126$, (c) $\overline{\epsilon} = -3.72$, $\Gamma = 0.308$, (d) $\overline{\epsilon} = -3.82$, $\Gamma = 0.94$, while thick lines are fits to a Gaussian with (e) $\overline{\epsilon} = -3.95$, $\Delta = 0.578$, and (f) $\overline{\epsilon} = -4.37$, $\Delta = 3.54$. In all cases $L = 18$ and $N = 6$.

cally in integrable systems [35, 36] through an analysis of states whose energy was in the center of the spectrum, i.e., whose $T_{CE} = \infty$. In order to make contact with the results in Refs. [35, 36], we compute $P(\epsilon)$ for our quenches and in the regions of the spectrum relevant to out work. Note that since full exact diagonalization is required to obtain all eigenstates $|\phi_n\rangle$, the largest systems considered here in the calculations of $P(\epsilon)$ have $L = 18$ and $N = 6$. Finite size effects are strong for those lattice sizes, so we average the results of $P(\epsilon)$ over the nine even parity states $|\psi_\alpha\rangle$ that are closest in energy to E_I

In Fig. 3, we show results of $P(\epsilon)$ for the same Hamiltonian parameters for which we previously studied the weighted energy densities. Comparing Fig. 3 and Fig. 2, one can see that the results for $P(\epsilon)$ and $P(E)$ are qualitatively similar. For both types of quenches, $P(\epsilon)$ becomes broader with increasing V (integrable) and $t' = V'$ (nonintegrable). However, when $\hat{H}_I$ is integrable, $P(\epsilon)$ remains better described by Breit-Wigner functions, while a transition from Breit-Wigner to Gaussian behavior, as well as a filling of the energy shell [better seen in Fig. 3(f) than in Fig. 2(f)], is only observed for a nonintegrable $\hat{H}_I$.

Our results for integrable systems are in contrast to those reported in Refs. [35, 36], where a transition from Breit-Wigner to Gaussian was also observed for an interaction quench within integrable systems. This can be attributed to the combination of two effects. One is the fact that the states $|\psi_\alpha\rangle$ selected here are far from the middle of the spectrum, the case in Ref. [35, 36]. Within the entire spectrum, the mean level spacing in the middle is the minimal one, i.e., the same perturbation may couple more states in that region than away from it. If the average level spacing is the only reason for the difference, then a transition should be seen in our case if one increases the system size.

However, there may be another reason which would make the differences remain in the thermodynamic limit. The result of averaging over eigenstates in the middle of the spectrum [35, 36] leads to an ensemble at infinite temperature. In that ensemble, the distribution of the quantities that are conserved after the quench could be featureless. This would result in an un-bias sampling of the eigenstates of the Hamiltonian after the quench, which may not occur for quenches starting at a finite temperature even if they are strong quenches. We have found this to be the case for quenches between hard-core boson systems in which one starts from a thermal state [12]. Only the initial state at the infinite temperature was found to ergodically sample the eigenstates after the quench, and a finite size scaling analysis showed that this remains true with increasing system size. We will come back to this point in Sec. VI, where the conserved quantities are studied for all quenches considered here.

V. ENTROPIES

The fact that the weighted energy density appears to be Gaussian after a quench to an integrable model does not automatically guarantee that thermalization will occur, as it does not mean that an un-bias sampling has been performed (unless the energy shell is filled). One needs to keep in mind that a coarse-graining is involved when calculating $P(E)$, where ΔE [see Eq. (12)] is much larger than the average level spacing. For example, in Ref. [12], we showed that quenches between integrable systems, which started from thermal states, led to Gaussian like weighted energy distributions that are not thermal and do not become thermal with increasing system size. The exception was the initial infinite temperature state, which does lead to a thermal distribution after a quench (but at infinite temperature). A qualitatively similar behavior was seen for quenches starting from special pure states that are ground states of an integrable Hamiltonian [11].

In order to quantify how the weights evolve in the DE as the system size increases, and how they compare to

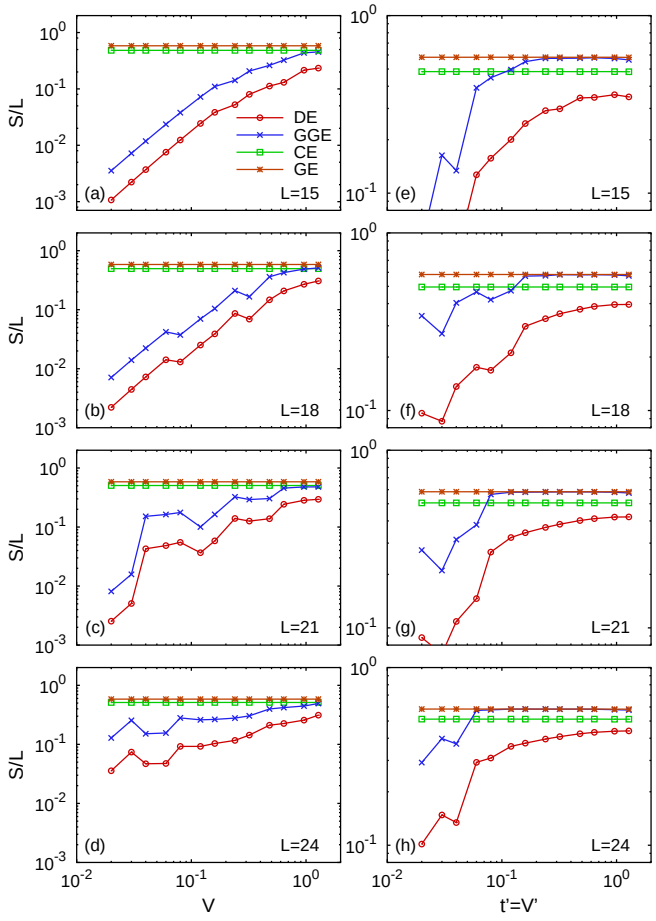

FIG. 4: (Color online) S/L for the DE, CE, GGE, and GE in systems with $L = 15$, 18, 21, and 24. Results are presented for (a)–(d) quenches type I and (e)–(h) quenches type II.

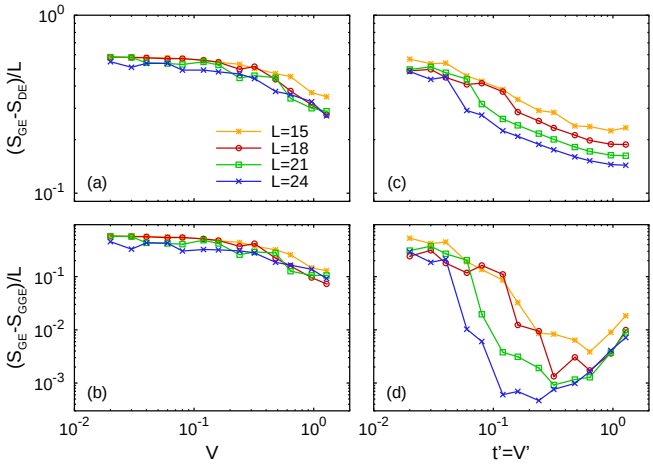

FIG. 5: (Color online) $(S_{\rm GE} - S_{\rm DE})/L$ as a function of (a) V for quench type I and (c) $t' = V'$ for quench type II. $(S_{\rm GE} - S_{\rm GGE})/L$ as a function of (b) V for quench type I and (d) $t' = V'$ for quench type II. Four different system sizes are presented for comparison.

the weights in the GGE, CE, and GE, we have computed the entropies of the corresponding ensembles for all the quenches studied before. In Fig. 4, we show all those entropies, per site, as a function of V for quenches type I [Figs. 4(a)–4(d)] and of $t' = V'$ for quenches type II [Figs. 4(e)–4(h)], for four system sizes. Since, in all cases, we consider a fixed effective temperature $T_{\rm CE} \approx 2$ after the quench, the values of S/L in the CE and the GE are (almost) independent of the quench parameters.

The first feature that is apparent in Fig. 4 is that, in both types of quenches, the entropy in the DE and the GGE are very small for weak quenches and increase with increasing quench strength. The GGE entropy follows (but is always above, as expected from its grand-canonical character) the DE entropy. In addition, for each quench, the difference between $S_{\rm DE}$, $S_{\rm GGE}$ and $S_{\rm CE}$, $S_{\rm GE}$ is seen to decrease with increasing system size. However, only in quench type II one can see $S_{\rm GGE}$ to become practically indistinguishable from $S_{\rm GE}$. If one agrees that the GGE describes observables after relaxation, then the agreement between $S_{\rm GGE}$ and $S_{\rm GE}$ implies that the observables thermalize in those quenches.

A better understanding of how the differences between entropies scale with increasing system size can be gained through Fig. 5. There we plot $(S_{\rm GE} - S_{\rm DE})/L$ and $(S_{\rm GE} - S_{\rm GGE})/L$ for different system sizes. Since $(S_{\rm GE} - S_{\rm CE})/L$ vanishes in the thermodynamic limit, we drop $S_{\rm CE}$ from the remaining analysis. We note that the analysis in Fig. 5 takes into account small fluctuations in $S_{\rm GE}$ (unnoticeable in Figs. 4) that occur because E_I is close but not identical in all initial states.

Figure 5 shows that, with increasing system size, a decrease of $(S_{\rm GE} - S_{\rm DE})/L$ and a vanishing of $(S_{\rm GE} - S_{\rm GGE})/L$ is apparent only in quenches type II, which, once again, indicates that thermalization will occur in those quenches. Furthermore, the value of $t' = V'$ at which an abrupt reduction of the differences $(S_{\rm GE} - S_{\rm DE})/L$ and $(S_{\rm GE} - S_{\rm GGE})/L$ occurs decreases as the system size increases, suggesting that in the thermodynamic limit an infinitesimally small type II quench will lead to thermalization. We should add that, in Fig. 5(d), the slight upturn (note the logarithmic scale in the y axes) of $(S_{\rm GE} - S_{\rm GGE})/L$ for the strongest quenches seems to be related to the skewing of the weighted energy density seen in Fig. 2. Its effect is imperceptible in Fig. 5(c), as $(S_{\rm GE} - S_{\rm DE})/L$ is more than an order of magnitude larger than $(S_{\rm GE} - S_{\rm GGE})/L$. From the evolution of the data with increasing size, we expect this upturn to disappear in the thermodynamic limit. For quenches type I, the results in Figs. 5(a) and 5(b) show that $(S_{\rm GE} - S_{\rm DE})/L$ and $(S_{\rm GE} - S_{\rm GGE})/L$, respectively, either remain finite in the thermodynamic limit or vanish very slowly with increasing system size.

VI. CONSERVED QUANTITIES

As mentioned before, the presence of nontrivial sets of conserved quantities make integrable systems different from nonintegrable ones. Hence, an understanding of whether a particular initial state leads to thermalization can also be gained from analyzing how the quantities that are conserved after the quench behave in the initial state. If the distribution of conserved quantities is identical to the one in thermal equilibrium with energy E_I after the quench, then the initial state can provide an un-bias sampling of the thermal one and lead to thermalization. Two particular examples in which that happens, in quenches between integrable systems, were discussed in Refs. [11, 12]. However, in those examples, the distributions of conserved quantities were featureless and corresponded to systems that were at infinite temperature after the quench.

In Fig. 6, we show the distribution of conserved quantities for various initial states for quenches type I [Figs. 6(a)–6(d)] and type II [Figs. 6(e)–6(h)], and compare them to the distribution of conserved quantities in the GE (which is almost identical in all quenches as E_I is very close in all of them). That figure shows that $\langle\Psi_I|\hat{I}_j|\Psi_I\rangle$ in quenches type I remains different from that in the CE for all values of V. In contrast, in type II quenches, $\langle\Psi_I|\hat{I}_j|\Psi_I\rangle$ becomes very similar to that in the CE as $t' = V'$ increase.

In order to have a more quantitative understanding of the difference between the conserved quantities in the initial state (in the GGE) and in the GE, as the system size increases, we calculate the relative integrated difference defined as

$$\Delta I = \frac{\sum_j |\langle\Psi_I|\hat{I}_j|\Psi_I\rangle - \langle\hat{I}_j\rangle_{\rm GE}|}{\sum_j \langle\Psi_I|\hat{I}_j|\Psi_I\rangle}. \qquad (16)$$

Results for ΔI in both types of quenches, and for different systems sizes, are presented in Fig. 6. They make

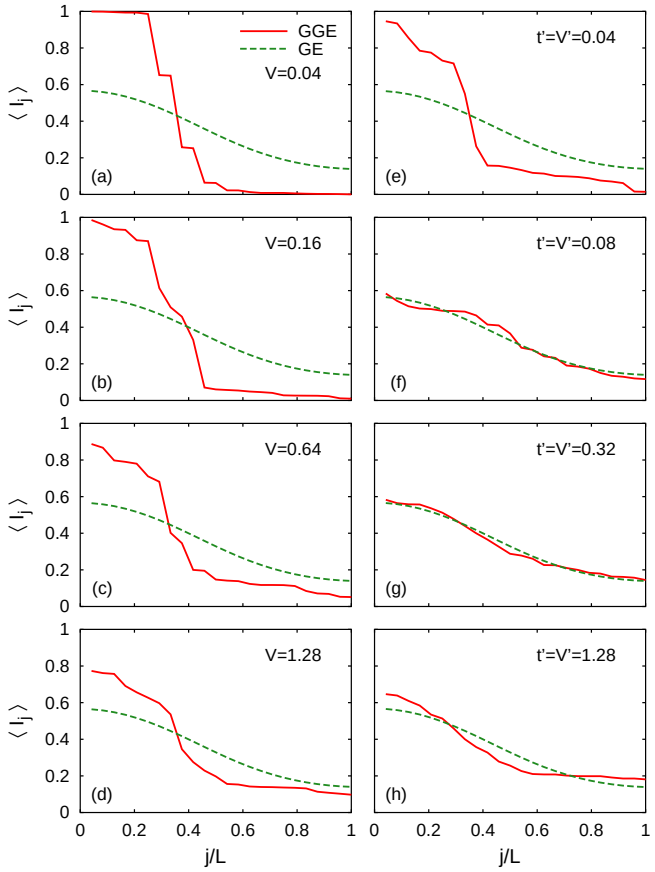

FIG. 6: (Color online) Distribution of conserved quantities $\langle\Psi_I|\hat{I}_j|\Psi_I\rangle$ in the initial state (same as the GGE) and in the GE. Results are presented for (a)–(d) type I quenches, and (e)–(h) type II quenches. In all cases, $L = 24$ and $N = 8$.

evident that, as the system size increases in quenches type II, the conserved quantities in the initial state converge to those predicted in thermal equilibrium. No such clear tendency is seen for quenches type I. We note that the results for ΔI are qualitatively similar to those obtained for $(S_{\rm GE} - S_{\rm GGE})/L$ in Fig. 7. This can be understood as the entropy in the initial state (GGE) and in the GE can be written in terms of the occupation of the single-particle eigenstates in each case

$$S = -\sum_{j=1}^{L}[(1 - I_j)\ln(1 - I_j) + I_j \ln I_j], \qquad (17)$$

where $I_j = \langle\Psi_I|\hat{I}_j|\Psi_I\rangle$ for the initial state (GGE) and $I_j = \langle\hat{I}_n\rangle_{\rm GE}$ for the GE.

The results obtained for quenches type II are remarkable as they imply that such quenches lead to thermalization in integrable systems. This occurs even though the distribution of conserved quantities is a nontrivial one (it is not flat, which was the case in Refs. [11, 12]). Beyond its implication for the quantum dynamics of integrable systems, one could think of using this information to learn about complicated many-body systems. It implies, e.g., that if we know the kinetic energy of a chaotic strongly correlated fermionic system in equilibrium, we could automatically calculate its momentum distribution by computing the momentum distribution function of a system that is in thermal equilibrium in the noninteracting limit with the same energy as the kinetic energy of the strongly correlated one.

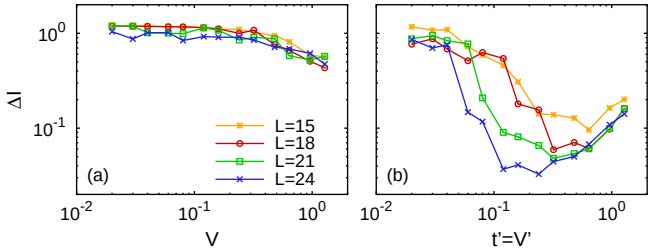

FIG. 7: (Color online) Relative integrated difference of the conserved quantities in the initial state (in the GGE) and the GE, ΔI, as a function of (a) V for quench type I and (b) $t' = V'$ for quench type II. Results are presented for four system sizes.

VII. MOMENTUM DISTRIBUTIONS

In this section, we test whether the conclusion reached in the previous sections, that quenches type I do exhibit a clear tendency to thermalize with increasing system size while quenches type II do, holds for an observable, the momentum distribution function m_k.

In Fig. 8, we show the momentum distribution function for the diagonal ensemble in various initial states for quenches type I [Figs. 8(a)–8(d)] and type II [Figs. 8(e)–8(h)], and compare them to the momentum distribution functions predicted by the GGE and the GE. That figure shows that while the GGE results closely follow the ones in the DE for all quenches, the CE results are only consistently closer to the DE ones in quenches type II as one increases $t' = V'$ [Figs. 8(f)–8(h)].

Once again, in order to be more quantitative, we compute the integrated differences between the GE and DE results, namely

$$\Delta m_{\rm DE} = \frac{\sum_k |\langle\hat{m}_k\rangle_{\rm GE} - \langle\hat{m}_k\rangle_{\rm DE}|}{\sum_k \langle\hat{m}_k\rangle_{\rm GE}}. \qquad (18)$$

Results for $\Delta m_{\rm DE}$ are presented in Fig. 9(a) for quenches type I and in Fig. 9(b) for quenches type II. In the former figure, no consistent trend is seen in the $\Delta m_{\rm DE}$ with increasing system size. In contrast, in Fig. 9(b) one can see that, for the three largest system sizes, $\Delta m_{\rm DE}$ decreases steadily with increasing L for $t' = V'$ between 0.1 and 1. This is in agreement with what was expected from our previous analyses, and indicates that quenches type II lead to thermalization for this observable, while quenches type I do not lead to thermalization or require

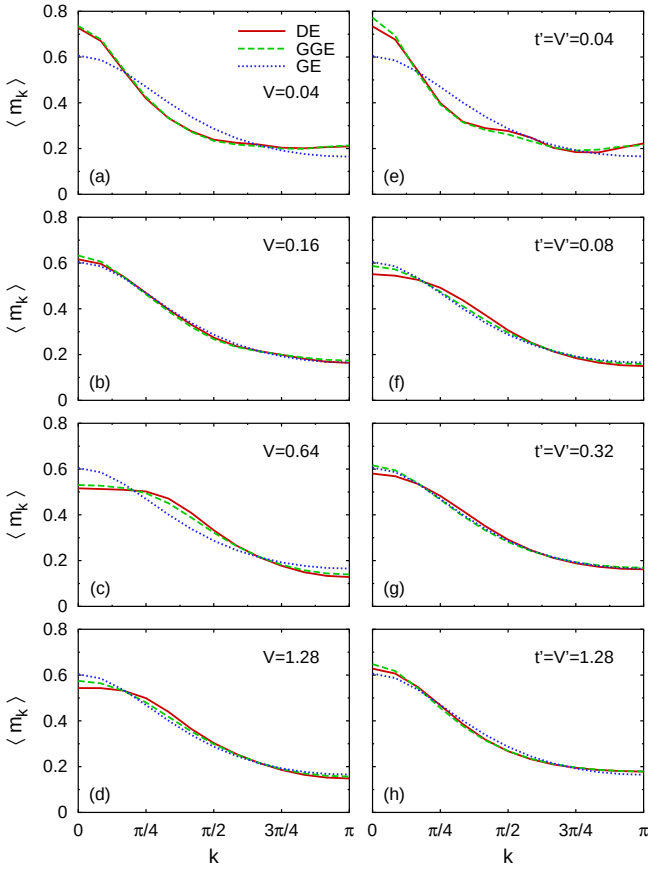

FIG. 8: (Color online) Momentum distribution functions in the DE, GGE, and GE. Results are presented for (a)–(d) type I quenches, and (e)–(h) type II quenches. In all cases, $L = 24$ and $N = 8$.

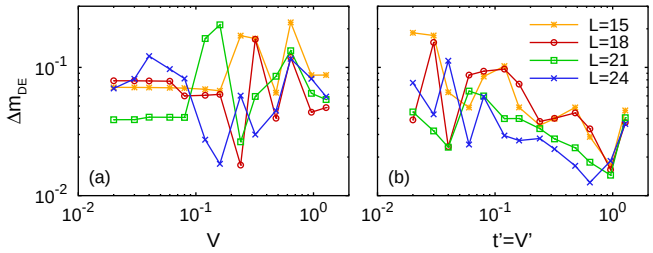

FIG. 9: (Color online) Relative integrated difference $\Delta m_{\rm DE}$ as a function of (a) V for quench type I and (b) $t' = V'$ for quench type II. Results are presented for four system sizes.

much larger system sizes to observe an approach to the thermal predictions.

VIII. SUMMARY

We have studied quenches to an integrable Hamiltonian (mappable to free fermions) in which the initial state is selected to be either an eigenstate of an integrable Hamiltonian that is non-mappable to a free model (quench type I) or an eigenstate of a nonintegrable one (quench type II). By studying weighted energy densities and entropies, we have not found clear evidence that quenches type I, at least within our Hamiltonians of interest and away from the middle of the spectrum, lead to an un-bias sampling of the eigenstates of the final Hamiltonian. Quenches type II, on the other hand, are found to provide such an un-bias sampling. Furthermore, an analysis of different systems sizes indicates that, in the thermodynamic limit, an infinitesimal quench type II will lead to thermalization. Here, an important requirement to keep in mind is that the initial state must be away from the edges of the spectrum. This is because, for systems in the absence of randomness and with two-body interaction, chaotic eigenstates can only be found away from the edges of the spectrum [33, 34].

We have also shown that, in the initial state, an analysis of the distribution of the quantities that are conserved after the quench provides an understanding of why thermalization occurs in one type of quenches while it fails in the other one. In quenches type I, that distribution remains different from, or approaches very slowly with increasing systems size, the one in thermal equilibrium after the quench. This implies that an un-bias sampling of the eigenstates of the final Hamiltonian does not occur or takes very large systems to be discerned. The opposite is true for quenches type II. Hence, quenches type II provide a consistent way of creating initial states that have the right distribution of conserved quantities so that thermalization can occur after a quench to integrability. Special initial states for which this occurred in quenches type I were discussed in Refs. [11, 12]. However, the distribution of conserved quantities in those cases was (trivially) flat corresponding to infinite temperature systems after the quench.

Finally, by studying the momentum distribution function in quenches type I and type II, we have shown that the conclusions reached on the basis of the results for the energy distributions, entropies, and conserved quantities hold. Namely, we have found no indications that quenches type I lead to the thermalization of this observable while quenches type II do result in thermal behavior.

Acknowledgments

This work was supported by the U.S. Office of Naval Research. We are grateful to F. M. Izrailev and L. F. Santos for useful comments on the manuscript.

[1] M. A. Cazalilla, R. Citro, T. Giamarchi, E. Orignac, and M. Rigol, Rev. Mod. Phys. **83**, 1405 (2011).
[2] T. Kinoshita, T. Wenger, and D. Weiss, Nature **440**, 900 (2006).
[3] M. Gring, M. Kuhnert, T. Langen, T. Kitagawa, B. Rauer, M. Schreitl, I. Mazets, D. A. Smith, E. Demler, and J. Schmiedmayer, Science **337**, 1318 (2012).
[4] S. Trotzky, Y.-A. Chen, A. Flesch, I. P. McCulloch, U. Schollwöck, J. Eisert, and I. Bloch, Nature Phys. **8**, 325 (2012).
[5] M. Rigol, V. Dunjko, and M. Olshanii, Nature **452**, 854 (2008).
[6] M. Rigol, Phys. Rev. Lett. **103**, 100403 (2009).
[7] M. Rigol, Phys. Rev. A **80**, 053607 (2009).
[8] M. Rigol, V. Dunjko, V. Yurovsky, and M. Olshanii, Phys. Rev. Lett. **98**, 050405 (2007).
[9] M. Rigol, A. Muramatsu, and M. Olshanii, Phys. Rev. A **74**, 053616 (2006).
[10] A. C. Cassidy, C. W. Clark, and M. Rigol, Phys. Rev. Lett. **106**, 140405 (2011).
[11] M. Rigol and M. Fitzpatrick, Phys. Rev. A **84**, 033640 (2011).
[12] K. He and M. Rigol, Phys. Rev. A **85**, 063609 (2012).
[13] M. A. Cazalilla, Phys. Rev. Lett. **97**, 156403 (2006).
[14] A. Iucci and M. A. Cazalilla, Phys. Rev. A **80**, 063619 (2009).
[15] A. Iucci and M. A. Cazalilla, New J. Phys. **12**, 055019 (2010).
[16] M.-C. Chung, A. Iucci, and M. A. Cazalilla, New J. Phys. **14**, 075013 (2012).
[17] P. Calabrese and J. Cardy, J. Stat. Mech. p. P06008 (2007).
[18] M. Kollar and M. Eckstein, Phys. Rev. A **78**, 013626 (2008).
[19] M. Cramer, C. M. Dawson, J. Eisert, and T. J. Osborne, Phys. Rev. Lett. **100**, 030602 (2008).
[20] T. Barthel and U. Schollwöck, Phys. Rev. Lett. **100**, 100601 (2008).
[21] D. Rossini, A. Silva, G. Mussardo, and G. E. Santoro, Phys. Rev. Lett. **102**, 127204 (2009).
[22] D. Rossini, S. Suzuki, G. Mussardo, G. E. Santoro, and A. Silva, Phys. Rev. B **82**, 144302 (2010).
[23] J. Mossel and J.-S. Caux, New J. Phys. **12**, 055028 (2010).
[24] D. Fioretto and G. Mussardo, New J. Phys. **12**, 055015 (2010).
[25] P. Calabrese, F. H. L. Essler, and M. Fagotti, Phys. Rev. Lett. **106**, 227203 (2011).
[26] P. Calabrese, F. H. L. Essler, and M. Fagotti, J. Stat. Mech. **2012**, P07022 (2012).
[27] P. Calabrese, F. H. L. Essler, and M. Fagotti, J. Stat. Mech. **2012**, P07016 (2012).
[28] E. T. Jaynes, Phys. Rev. **106**, 620 (1957).
[29] E. T. Jaynes, Phys. Rev. **108**, 171 (1957).
[30] J. M. Deutsch, Phys. Rev. A **43**, 2046 (1991).
[31] M. Srednicki, Phys. Rev. E **50**, 888 (1994).
[32] M. Rigol and M. Srednicki, Phys. Rev. Lett. **108**, 110601 (2012).
[33] L. F. Santos and M. Rigol, Phys. Rev. E **81**, 036206 (2010).
[34] L. F. Santos and M. Rigol, Phys. Rev. E **82**, 031130 (2010).
[35] L. F. Santos, F. Borgonovi, and F. M. Izrailev, Phys. Rev. Lett. **108**, 094102 (2012).
[36] L. F. Santos, F. Borgonovi, and F. M. Izrailev, Phys. Rev. E **85**, 036209 (2012).
[37] V. V. Flambaum, F. M. Izrailev, and G. Casati, Phys. Rev. E **54**, 2136 (1996).
[38] V. V. Flambaum and F. M. Izrailev, Phys. Rev. E **55**, R13 (1997).
[39] V. V. Flambaum and F. M. Izrailev, Phys. Rev. E **56**, 5144 (1997).
[40] V. V. Flambaum and F. M. Izrailev, Phys. Rev. E **61**, 2539 (2000).
[41] T. Holstein and H. Primakoff, Phys. Rev. **58**, 1098 (1940).
[42] P. Jordan and E. Wigner, Z. Phys. **47**, 631 (1928).
[43] M. Rigol and A. Muramatsu, Phys. Rev. A **70**, 031603(R) (2004).
[44] M. Rigol and A. Muramatsu, Phys. Rev. A **72**, 013604 (2005).
[45] K. He and M. Rigol, Phys. Rev. A **83**, 023611 (2011).
[46] M. Rigol, Phys. Rev. A **72**, 063607 (2005).
[47] H. Fang and Y. Saad, SIAM Journal on Scientific Computing **34**, A2220 (2012).
[48] A. Polkovnikov, Ann. Phys. **326**, 486 (2011).
[49] L. Santos, A. Polkovnikov, and M. Rigol, Phys. Rev. Lett. **107**, 40601 (2011).
[50] M. Rigol, Phys. Rev. A **82**, 037601 (2010).